American Mineralogist, Volume 69, pages 176–185, 1984

Crystal structure of ilmenite ($FeTiO_3$) at high temperature and at high pressure

BARRY A. WECHSLER[1] AND CHARLES T. PREWITT

Department of Earth and Space Sciences
State University of New York
Stony Brook, New York 11794

Abstract

The structures of two single crystals of synthetic ilmenite were refined using X-ray intensity data collected at 24, 400, 600, 800, and 1050°C (1 atm) and 0.001, 25.4, 34.6, and 46.1 kbar (room temperature). Thermal expansion of the unit cell was nearly isotropic, whereas compression was relatively anisotropic, with *c/a* decreasing linearly with increasing pressure. The isothermal bulk modulus and its pressure derivative determined from cell volume data are K_o = 1.70(7) Mbar, K_o' = 8(4), or K_o = 1.77(3) if K_o' is assumed to be 4(1). Mean Fe–O and Ti–O distances increased linearly with temperature and decreased linearly with pressure, ⟨Fe–O⟩ being about twice as expandable and compressible as ⟨Ti–O⟩. The responses of the two octahedral sites to temperature and pressure were quite different from one another, however. The longer of the two independent Fe–O bonds was more expandable and less compressible than the shorter one, whereas the opposite was true for the Ti site. The Ti atom was displaced toward the centroid of its coordination polyhedron at high temperature, but the Fe atom moved further away from its centroid position. Cation shifts were much smaller with pressure than with temperature. These results indicate that the reponses of the ilmenite structure to temperature and pressure are not inverse in character. The cation sites remained fully ordered at all temperatures and pressures studied.

Introduction

Ilmenite ($FeTiO_3$) occurs as an accessory mineral in a wide variety of igneous and metamorphic rocks (Haggerty, 1976; El Goresy, 1976a,b; Rumble, 1976). One of its most valuable characteristics for petrogenetic studies has been the use of compositions of coexisting hematite–ilmenite and magnetite–ulvöspinel solid solutions as an indicator of temperature and oxygen fugacity at the time of last equilibration (Lindsley, 1963; Buddington and Lindsley, 1964). More recently, other geothermometers have been based upon coexisting ilmenite and olivine or pyroxene (Andersen and Lindsley, 1979; Bishop, 1980) and have utilized solution models to extend the experimental calibrations. The ilmenite structure may also be an important one for metasilicates undergoing high-pressure transformations in the Earth's mantle (*e.g.*, Ringwood, 1969; Liu, 1977a). In order to improve thermochemical models, understand crystal-chemical partitioning behavior, and characterize the pressure–temperature systematics of compounds with the ilmenite structure, it would be useful to determine the effects of elevated temperature and pressure upon the crystal structure of ilmenite.

The ilmenite structure was determined by Barth and Posnjak (1934). Shirane *et al.* (1959) determined the magnetic structure at low temperature using neutron diffraction, and the structure of lunar ilmenite was studied by Raymond and Wenk (1971). Numerous other investigations have elucidated the magnetic properties of ilmenites and hematite–ilmenite solutions (*e.g.*, Ishikawa, 1958, 1962; Shirane and Ruby, 1962; Shirane *et al.*, 1962; Thorpe *et al.*, 1977) and have suggested the possibility of an order–disorder transformation at high temperatures as is observed for intermediate compositions. Burton (1980) studied such a transformation in an intermediate hematite–ilmenite by single-crystal X-ray diffraction.

Recently, high-pressure structure refinements have been reported for several materials with the closely related corundum structure (Finger and Hazen, 1980). Compression of ilmenite has also previously been studied by X-ray diffraction (Liu *et al.*, 1974) and Mössbauer spectroscopy (Vaughan and Drickamer, 1967) on polycrystalline specimens. A number of other studies have considered the elasticity, crystal-chemical systematics, and high-pressure phase transformations in other compounds possessing the ilmenite structure (Liebermann,

[1] Present address: Hughes Research Laboratories, 3011 Malibu Canyon Road, Malibu, California 90265.

0003–004X/84/0102–0176$02.00

1976; Liu, 1977b; Kirfel *et al.*, 1978; Ito and Matsui, 1979).

The present study was undertaken to characterize changes in the crystal structure of ilmenite with temperature and under isothermal, hydrostatic compression and to compare this behavior with that found for similar materials.

Experimental procedures

Synthesis of samples

The ilmenite used in this study was synthesized by D. H. Lindsley (run no. L679). The starting material was a stoichiometric mix of Fe + Fe_2O_3 + TiO_2. It was loaded dry into a Ag capsule and reacted in a piston-cylinder apparatus at 20 kbar, 1000°C for 1 day, 22 hours. The run products consisted of single crystals of ilmenite, generally equant and subhedral, ~50-150 μm in diameter.

Precession camera studies

A single crystal cemented to a quartz glass fiber and sealed in an evacuated silica capillary was studied at high temperature on a precession camera. Precession photos of the *h0l* orientation were exposed for ~24 hours each at 500, 700, 900, 1000, and 1150°C. Three relatively weak but observable reflections which are allowed in space group $R\bar{3}$ but forbidden in $R\bar{3}c$ were found to be present at all temperatures. The reflections monitored were $\bar{2}01$, 107, and 205, which are excluded by the condition $l = 2n$ in $R\bar{3}c$. This evidence precludes the possibility of a space group transformation from $R\bar{3}$ to $R\bar{3}c$, which would be indicative of complete cation disorder, to 1150±20°C. No decomposition or loss of resolution in diffraction spots was observed throughout the heating experiment.

High temperature data collection

Another ilmenite crystal from the same synthesis run was studied at high temperature on an automated four-circle diffractometer. Three-dimensional X-ray intensity data were collected at 24, 400, 600, 800, and 1050°C, and again at room temperature after heating (RTAH). The crystal was held at temperature for 3 to 4 hours before data collection was begun. All reflections with two theta less than 70° for graphite-monochromated Mo$K\alpha$ radiation were measured. At room temperature, data were collected in a hemisphere of reciprocal space, while at high temperatures, only one quadrant of reciprocal space was studied in order to minimize the total exposure at high temperature. Intensity data were converted to structure factors by correcting for background and Lorentz-polarization factors. Following the collection of intensity data at each temperature, 2θ values of from 12 to 15 reflections were measured, and the average of the positive and negative 2θ values was used in a least-squares refinement of the unit-cell parameters (Table 1).

Table 1. Unit-cell parameters of ilmenite at high temperature

T(°C)	a(Å)	c(Å)	V(Å^3)	c/a
24	5.0884(1)*	14.0855(4)	315.84(1)	2.7682
400	5.1080(1)	14.1287(6)	319.25(1)	2.7660
600	5.1182(1)	14.1566(6)	321.16(1)	2.7659
800	5.1280(1)	14.187(1)	323.08(3)	2.7666
1050	5.1412(1)	14.2250(6)	325.62(1)	2.7669
RTAH**	5.0889(1)	14.0933(5)	316.08(1)	2.7694

* *Standard deviations are given in parentheses and refer to the estimated error in the least significant units. This convention is followed in all tables.*

** *Room temperature after heating.*

High pressure data collection

A third crystal from the same synthesis run was selected for high pressure study. Precession and Weissenberg photos showed the sample to be a single crystal with sharp diffraction spots.

Three-dimensional X-ray intensity data were collected at room temperature and pressure. All reflections with 2θ less than 70° were measured in one hemisphere of reciprocal space. Structure refinement based on these data (see below) yielded essentially identical parameters to those obtained from the crystal used for high-temperature study. The crystal was then placed in a Merrill and Bassett-type miniature opposed anvil diamond cell (Merrill and Bassett, 1974) for high pressure diffraction measurements. An Inconel X-750 gasket was used (0.25 mm thickness) with a 0.35 mm hole for the sample chamber. The crystal was attached to one diamond face with a small amount of the alcohol-insoluble fraction of petroleum jelly, which partially covered a portion of the crystal. The pressure-transmitting medium was a 4:1 mixture of methanol:ethanol (Piermarini *et al.*, 1973). A ruby crystal ~30 μm in diameter was placed in the sample chamber to monitor the pressure. Pressure was calibrated by measuring the shift of the R_1 ruby fluorescence line (Barnett *et al.*, 1973; Piermarini *et al.*, 1975; King and Prewitt, 1980). The estimated precision of the pressure determination is ±0.5 kbar. Pressure was determined immediately after loading the diamond cell at each pressure and again following data collection. In general, at least 24–48 hours elapsed between loading and the start of data collection, during which time some relaxation occurred. The pressures quoted for each experiment were those determined following the completion of data collection.

Initial loading was at 12.2 kbar, followed by data collection at 25.4 kbar. After this, the diamond cell was opened to move the crystal back to the center of the gasket hole. Following data collection at 34.6 kbar, the cell was again opened to move the crystal back to the center. Because of the thickness of the gasket at 12 kbar, a significant amount of shielding of the X-ray beam occurred. Therefore, the refinements at this pressure will not be considered further here. However, the unit-cell

determination at this pressure appears quite good. Subsequent data collection at higher pressures was only minimally affected by gasket cutoff, resulting in a relatively small number of reflections which were excluded from the refinements.

Intensity data were collected in the fixed-phi mode and intensities were measured using the constant-precision scanning technique (Finger *et al.*, 1973). All accessible reflections with 2θ less than 90° in a sphere of reciprocal space were collected. Due to the unfavorable orientation of the crystal at 35 and 46 kbar, only reflections with small values of l could be measured, resulting in the relatively large uncertainties in the z coordinates for these refinements. All intensities were corrected for absorption due to the diamond and beryllium in the pressure cell, using the method described by Finger and King (1978).

Unit-cell parameters were determined at both room pressure and at high pressures from the settings for 20–24 centered reflections corrected for errors in crystal centering and diffractometer zeroes using the procedures of King and Finger (1979). The triclinic cell, with no constraints, was in every case consistent with rhombohedral symmetry, suggesting that hydrostatic stress was maintained during data collection. Unit-cell parameters are reported in Table 2.

Precession photos of the crystal were taken in both $h0l$ and $hk0$ orientations following high-pressure data collection. These suggest no deterioration of the crystal as a result of compression nor was there any indication of twinning as has been observed in shock-compressed ilmenites (Sclar *et al.*, 1973).

Absorption correction

Absorption corrections were applied to all intensity data using linear absorption coefficients varying from 106.3 to 103.1 cm^{-1} for the high-temperature data and 106.3 to 109.0 cm^{-1} for the high-pressure data. The crystals studied at high temperature and high pressure measured ~0.06 × 0.08 × 0.12 mm and ~0.05 × 0.07 × 0.10 mm, respectively. Extinction factors were also calculated for all reflections. Although it would have been better to use a constant absorption coefficient for all data sets, we are confident that this inadvertent error has not significantly affected the final results. Examination of the transmission and extinction factors indicates that the principal effect of varying the absorption coefficient was a simple scaling, by a maximum of 2–3% for transmission and 5–7% for extinction factors. The deviations in individual structure factors not accounted for by the overall scale factor and extinction parameter (r*) are smaller than other sources of statistical uncertainties in the data.

Table 2. Unit-cell parameters of ilmenite at high pressure

P(kbar)	a(Å)	c(Å)	V(Å^3)	c/a
0.001	5.0875(5)*	14.0827(7)	315.68(4)	2.7681
12.2	5.0785(5)	14.0358(17)	313.50(6)	2.7638
25.4	5.0691(4)	13.9849(13)	311.21(4)	2.7589
34.6	5.0635(2)	13.9518(16)	309.79(4)	2.7554
46.1	5.0561(4)	13.9115(19)	307.99(5)	2.7514

Standard deviations are given in parentheses and refer to the estimated error in the least significant units. This convention is followed in all tables.

All reflection data were averaged prior to refinement to produce a set of symmetry-independent reflections. For the high-pressure data, a number of reflections that differed significantly from their equivalents were omitted prior to averaging.

Structure refinements

Structure refinements were carried out using the least-squares program RFINE4 (Finger and Prince, 1975). Starting coordinates were taken from Shirane *et al.* (1962), and the neutral atom scattering factors of Doyle and Turner (1968) were used. Real and imaginary parts of the anomalous dispersion corrections were also included for all atoms. Reflections were weighted on the basis of counting statistics, and those with $F < 3\sigma_F$ (high temperature) or $I < 2\sigma_I$ (high pressure) were excluded from the refinements. A scale factor, positional parameters, isotropic or anisotropic temperature factors, and an isotropic secondary extinction correction were varied in the final cycles of refinement. Final values of refined parameters are reported in Tables 3 and 4. Final observed and calculated structure factors for all data sets are listed in Table 5.[2] Selected interatomic distances and angles (uncorrected for thermal motion) and coefficients of expansion and compression are given in Tables 6 and 7.

In the final cycles of refinement of the high-temperature data, the weighting scheme of Prince (1978) was employed. Although none of the refined parameters changed significantly as a result of this weighting scheme, the statistical parameters were improved. Also, from 3 to 5 observed reflections were rejected from each refinement on the basis of very high delta/sigma values. It is believed that these reflections may have been affected by "powder rings" arising from recrystallization of the high-temperature cement holding the crystal in place. For the high-pressure data, a few reflections having large delta/sigma values believed to have been affected by gasket cutoff were excluded.

The 35 kbar refinement is the most uncertain of the high-pressure results. The Fe atom z coordinate in this refinement is particularly anomalous, lying off the trend defined by the 1 atm, 25 and 46 kbar results by about 3 esd. This may have resulted from the unfavorable orientation of the crystal during data collection at this pressure, which was limited to reflections with l less than or equal to 5.

[2] To receive a copy of Table 5, order Document AM-83-235 from the Business Office, Mineralogical Society of America, 2000 Florida Avenue, N. W., Washington, D. C. 20009. Please remit $5.00 in advance for the microfiche.

Table 3. Final positional parameters and isotropic temperature factors (Å^2) of ilmenite at high temperature

		24°C	400°C	600°C	800°C	1050°C	RTAH
Fe	x	0	0	0	0	0	0
	y	0	0	0	0	0	0
	z	0.35537(2)	0.35605(3)	0.35650(4)	0.35689(5)	0.35732(6)	0.35542(2)
	B	0.582(8)	1.17(1)	1.51(1)†	1.86(2)†	2.37(2)†	0.57(1)
Ti	x	0	0	0	0	0	0
	y	0	0	0	0	0	0
	z	0.14640(2)	0.14676(4)	0.14696(4)	0.14722(5)	0.14748(6)	0.14645(3)
	B	0.458(7)	0.87(1)	1.10(1)†	1.32(1)†	1.61(2)†	0.47(1)
O	x	0.31743(18)	0.31796(29)	0.31864(34)	0.31919(39)	0.31867(44)	0.31745(26)
	y	0.02332(17)	0.02432(28)	0.02438(34)	0.02499(36)	0.02491(43)	0.02345(25)
	z	0.24506(5)	0.24479(8)	0.24479(11)	0.24496(13)	0.24475(16)	0.24485(7)
	B	0.58(1)†	1.06(2)†	1.31(2)†	1.65(3)†	1.99(3)†	0.58(2)†
r*	(x10^5)††	1.09(5)	0.96(6)	0.83(6)	0.84(7)	1.05(8)	0.46(4)
N(obs)		285	253	255	245	248	271
R(wt)		0.015	0.020	0.024	0.026	0.028	0.020
R		0.019	0.028	0.036	0.038	0.047	0.024

† *Equivalent isotropic B.*
†† *Secondary extinction parameter.*

Results

Unit-cell parameters

Thermal expansion was nearly isotropic between room temperature and 1050°C. The *a* cell dimension increased linearly with temperature, whereas *c* and the cell volume appeared to increase somewhat more rapidly at high temperature than at lower temperatures. However, because our methods for determining lattice parameters of this crystal did not explicitly take account of possible errors in crystal orientation and centering, the reported uncertainties are probably underestimated. It is likely that the true standard deviations of the high-temperature cell parameters are on the order of five times those reported, and possibly more. Therefore, we cannot be confident about the curvature in the *c*-dimension with temperature. A small increase was noted in *c* determined at room temperature after heating. This may have been due to misalignment of the crystal and is not believed to be indicative of any structural changes resulting from heating.

Table 4. Final positional parameters and isotropic temperature factors (Å^2) of ilmenite at high pressure

		1 atm	25.4 kbar	34.6 kbar	46.1 kbar
Fe	x	0	0	0	0
	y	0	0	0	0
	z	0.35540(1)	0.35562(3)	0.35530(14)	0.35580(11)
	B	0.625(8)†	0.68(2)	0.63(2)	0.63(2)
Ti	x	0	0	0	0
	y	0	0	0	0
	z	0.14638(2)	0.14637(4)	0.14650(19)	0.14644(14)
	B	0.505(8)†	0.53(1)	0.50(2)	0.52(2)
O	x	0.31719(11)	0.31596(30)	0.31657(36)	0.31649(32)
	y	0.02340(12)	0.02301(27)	0.02284(29)	0.02165(26)
	z	0.24502(4)	0.24537(11)	0.24520(28)	0.24545(25)
	B	0.62(1)†	0.61(2)	0.63(3)	0.65(3)
r* (x10^5)††		2.27(10)	2.28(16)	1.36(15)	1.32(12)
N(obs)		308	140	75	91
R(wt)		0.022	0.023	0.022	0.020
R		0.015	0.020	0.019	0.019

† *Equivalent isotropic B.*
†† *Secondary extinction parameter.*

The *c* cell dimension in ilmenite was approximately twice as compressible as *a* between 1 atm and 46 kbar. The compression in both directions was curvilinear, decreasing slightly with increased pressure, while the *c*/*a* ratio decreased linearly.

The volume compression data were fit to a Birch-Murnaghan equation of state (Bass *et al.*, 1981), in order to determine the zero-pressure isothermal bulk modulus and its pressure derivative. Since no rigorous constraint on K_o' is available, both K_o and K_o' were varied, yielding K_o = 1.70(7) Mbar and K_o' = 8(4). However, if K_o' is assumed to be 4(1) (see discussion below), the derived value of K_o = 1.77(3) Mbar. (The assumed uncertainty in K_o' was included in calculating the uncertainty of K_o.) This compares well with values determined for a natural single crystal of ilmenite, K_o = 1.79 Mbar (Madelung and Fuchs, 1921; Birch, 1966), and on a polycrystalline specimen of magnesian ilmenite, K_o = 1.68(12) Mbar (Liu *et al.*, 1974). It is also in good agreement with the bulk modulus *vs.* molar volume systematics for ilmenite-type compounds (Liebermann, 1976), which suggest K = 1.74 Mbar for $FeTiO_3$ (R. C. Liebermann, pers. comm.).

Structural changes

The ilmenite structure is based on the R_2O_3 corundum structure in which oxygens form a nearly hexagonal close-packed framework. Layers of edge-sharing octahedral cation sites extend in the (001) planes. Each cation shares one octahedral face with a cation in an adjacent layer, whereas the face opposite this is "shared" with a

Table 6. Selected interatomic distances (Å), angles (°), and thermal expansion coefficients of ilmenite at high temperature

	24°C	400°C	600°C	800°C	1050°C	RTAH	α*
Fe-O	2.2013(8)	2.219(1)	2.230(2)	2.238(2)	2.248(2)	2.204(1)	20.6
Fe-O	2.0778(8)	2.086(1)	2.086(2)	2.088(2)	2.093(2)	2.080(1)	7.1
<Fe-O>	2.1396	2.152	2.158	2.163	2.171	2.142	14.3
Ti-O	2.0886(8)	2.090(1)	2.095(1)	2.100(2)	2.099(2)	2.087(1)	4.8
Ti-O	1.8744(8)	1.879(1)	1.882(2)	1.885(2)	1.892(2)	1.874(1)	9.1
<Ti-O>	1.9815	1.985	1.988	1.993	1.996	1.980	7.1
QE**(Fe)	1.0271	1.0285	1.0292	1.0300	1.0311	1.0272	
QE (Ti)	1.0277	1.0273	1.0267	1.0262	1.0259	1.0278	
FeO_6 vol. (Å^3)	12.562	12.766	12.855	12.930	13.052	12.604	
TiO_6 vol. (Å^3)	10.001	10.051	10.119	10.191	10.238	9.978	
Fe-Ti	2.9435(4)	2.9570(7)	2.9663(8)	2.975(1)	2.985(1)	2.9450(5)	13.7
Fe-Fe 1†	3.0027(1)	3.0182(2)	3.0269(3)	3.0352(3)	3.0457(4)	3.0033(2)	14.0
Fe-Fe 2	4.0744(4)	4.0677(6)	4.063(1)	4.061(1)	4.059(1)	4.0752(4)	-3.6
Ti-Ti 1	2.9928(1)	3.0023(2)	3.0072(2)	3.0117(3)	3.0180(3)	2.9928(2)	8.2
Ti-Ti 2	4.1242(4)	4.1471(8)	4.161(1)	4.177(1)	4.196(1)	4.1279(6)	17.0
O-O 1††	2.701(1)	2.712(2)	2.723(3)	2.731(3)	2.734(3)	2.701(2)	11.9
O-O 2	3.216(1)	3.234(2)	3.238(3)	3.247(3)	3.257(3)	3.217(2)	12.4
O-O 3	3.051(1)	3.072(2)	3.080(3)	3.086(4)	3.098(4)	3.058(2)	15.0
O-O 4	3.005(1)	3.019(2)	3.023(3)	3.024(3)	3.038(4)	3.010(2)	10.7
O-O 5	2.921(1)	2.925(2)	2.927(3)	2.928(3)	2.939(3)	2.920(2)	6.0
O-O 6	2.607(1)	2.605(2)	2.611(3)	2.619(4)	2.620(4)	2.602(2)	4.9
O-O 7	2.885(1)	2.892(2)	2.896(3)	2.907(3)	2.911(4)	2.882(2)	8.8
O-Fe-O	75.68(3)	75.35(5)	75.26(6)	75.20(7)	74.88(8)	75.55(4)	
O-Fe-O	90.92(3)	91.02(5)	91.00(6)	90.95(7)	90.97(8)	91.03(4)	
O-Fe-O	89.15(4)	88.99(6)	88.87(8)	88.64(9)	88.7(1)	89.23(6)	
O-Fe-O	101.40(3)	101.65(4)	101.81(6)	102.07(7)	102.18(8)	101.32(4)	
O-Ti-O	80.56(3)	80.88(5)	81.06(7)	81.13(8)	81.26(9)	80.65(4)	
O-Ti-O	82.07(3)	81.84(5)	81.89(7)	81.97(8)	81.9(1)	81.97(4)	
O-Ti-O	93.28(4)	93.37(7)	93.33(9)	93.5(1)	93.5(1)	93.24(6)	
O-Ti-O	102.35(3)	102.26(5)	102.14(6)	101.88(7)	101.88(9)	102.40(4)	

*$\alpha = [(1/d_{24})(d_{1050}-d_{24})/1026] \times 10^6$ ($°C^{-1}$).
**Quadratic elongation.
†Metal-metal distances are indicated as follows:
1--across shared edge between adjacent metal sites; 2--across vacant octahedral position, along [001].
††Oxygen-oxygen distances are indicated as follows:
1--Fe-Ti shared face; 2--Fe site, face opposite the shared face; 3--Fe site, shared edge; 4--Fe site, unshared edge;
5--Ti site, face opposite the shared face; 6--Ti site, shared edge; 7--Ti site, unshared edge.

vacant octahedral position. In ilmenite, Fe and Ti are completely ordered into alternating layers along **c**, so that each cation shares three edges with other octahedral cations of the same type, but the common octahedral face is shared with a cation of the other type. On either side of each vacant octahedral position along **c** lie cations of the same type. Both cation sites lie on threefold axes, and each has a single variable positional parameter, z. Deviations of z from 1/3 and 1/6 for Fe and Ti sites, respectively, are indicative of "puckering" of the cation layers above and below planes parallel to (001).

The Fe and Ti atom z coordinates both increased linearly with temperature, corresponding to movement toward the centroid of the coordination polyhedron for Ti and away from the centroid position for Fe. "Puckering" of the Fe layer was significantly increased, and the Fe–Fe distance across the vacant octahedral site in the Ti layer actually decreased at high temperatures. The longer of the two independent Fe–O bonds increased nearly three times as rapidly as the shorter distance, whereas for the Ti atom, the shorter bond distance increased twice as rapidly as the longer one (see thermal expansion coefficients in Table 6). Thus, the FeO_6 octahedron became significantly more distorted at high temperature, while the TiO_6 octahedron became more regular, as indicated by the quadratic elongation (Robinson *et al.*, 1971; see Table 6). Mean Fe–O and Ti–O distances increased linearly with temperature, with ⟨Fe–O⟩ increasing about twice as much as ⟨Ti–O⟩ between 24 and 1050°C.

The fractional coordinate z of the Fe atom increased slightly with pressure, whereas the Ti z coordinate was unchanged. Small shifts were found for all three oxygen coordinates, with y changing the most and z the least with increasing pressure. The Fe and Ti sites were affected quite differently by compression. The longer of the two independent Fe–O distances was somewhat less compressible than the shorter Fe–O distance, whereas the longer Ti–O distance was more than twice as compressible as the shorter one (Table 7). However, overall distortions of the FeO_6 and TiO_6 polyhedra, as measured by the quadratic elongation and octahedral angle variance, were only slightly affected by pressure. Mean Fe–O and Ti–O distances decreased linearly with pressure, with the ⟨Fe–O⟩ distance about twice as compressible as ⟨Ti–O⟩.

Although the change in the oxygen z coordinate with pressure is small, it reflects the difference in behavior between the Fe and Ti sites. The octahedral height

Table 7. Selected interatomic distances (Å), angles (°), and coefficients of compressibility of ilmenite at high pressure

	1 atm	25.4 kbar	34.6 kbar	46.1 kbar	β*
Fe-O	2.2005(6)	2.184(1)	2.181(3)	2.180(3)	20.2
Fe-O	2.0784(5)	2.067(1)	2.065(2)	2.052(2)	27.6
<Fe-O>	2.1395	2.126	2.123	2.116	23.8
Ti-O	2.0871(5)	2.076(1)	2.072(3)	2.072(3)	15.7
Ti-O	1.8742(5)	1.872(1)	1.868(3)	1.869(2)	6.0
<Ti-O>	1.9806	1.974	1.970	1.970	11.6
QE**(Fe)	1.0272	1.0277	1.0268	1.0275	
QE (Ti)	1.0279	1.0279	1.0276	1.0272	
FeO_6 vol. (Å^3)	12.558	12.303	12.277	12.147	
TiO_6 vol. (Å^3)	9.984	9.881	9.829	9.839	
Fe-Ti	2.9436(4)	2.9263(8)	2.913(4)	2.913(3)	22.5
Fe-Fe 1†	3.0023(3)	2.9923(3)	2.9870(8)	2.9853(7)	12.3
Fe-Fe 2	4.0727(3)	4.038(1)	4.038(4)	4.012(3)	32.3
Ti-Ti 1	2.9923(3)	2.9812(3)	2.977(1)	2.9729(8)	14.1
Ti-Ti 2	4.1229(6)	4.094(1)	4.088(5)	4.074(4)	25.7
O-O 1††	2.698(1)	2.679(2)	2.682(3)	2.682(3)	12.9
O-O 2	3.217(1)	3.214(2)	3.200(2)	3.185(2)	21.6
O-O 3	3.051(1)	3.022(3)	3.020(7)	3.003(6)	34.1
O-O 4	3.005(1)	2.982(3)	2.979(7)	2.968(6)	26.7
O-O 5	2.921(1)	2.918(2)	2.912(2)	2.913(2)	5.9
O-O 6	2.604(1)	2.596(3)	2.590(7)	2.595(6)	7.5
O-O 7	2.884(1)	2.877(3)	2.866(6)	2.861(5)	17.3
O-Fe-O	75.61(2)	75.66(6)	75.88(14)	75.90(12)	
O-Fe-O	90.93(2)	90.56(6)	90.63(13)	90.33(11)	
O-Fe-O	89.18(3)	89.04(8)	89.06(13)	89.00(12)	
O-Fe-O	101.41(2)	101.76(6)	101.55(12)	101.82(11)	
O-Ti-O	80.53(2)	80.37(6)	80.65(14)	80.64(12)	
O-Ti-O	82.02(2)	82.06(6)	81.99(16)	82.19(14)	
O-Ti-O	93.31(3)	93.40(8)	93.19(13)	92.96(12)	
O-Ti-O	102.38(2)	102.39(6)	102.41(17)	102.41(14)	

*$\beta = -[(1/d_o)(d_{46.1}-d_o)/46.1] \times 10^5$ (kbar^{-1}).

**Quadratic elongation.

†Metal-metal distances are indicated as follows:
1 - across shared edge between adjacent metal sites;
2 - across vacant octahedral position, along [001].

††Oxygen-oxygen distances are indicated as follows:
1--Fe-Ti shared face; 2--Fe site, face opposite the shared face; 3--Fe site, shared edge; 4--Fe site, unshared edge; 5--Ti site, face opposite the shared face; 6--Ti site, shared edge; 7--Ti site, unshared edge.

(distance between upper and lower oxygen layers along **c**) is dependent upon the *c* length and the oxygen *z* coordinate. The slight increase in z_{oxy} with increasing pressure indicates that the octahedral height of the Fe layer probably decreases more than twice as rapidly as that of the Ti layer. This decrease is also more than twice the linear compressibility in the **a**-direction. Thus, the Fe site is "flattened" relative to the Ti site, which compresses about equally along **a** and **c**. This is perhaps the reason for the decrease in *c/a* with increasing pressure. The greater **c**-axis compression is, of course, also associated with more substantial shortening of metal–metal distances along **c** (*i.e.*, Fe-Ti across shared face, Fe–Fe and Ti–Ti across vacant sites) than between adjacent metal sites across shared edges.

Cation distribution

In order to determine whether any disorder between Fe and Ti sites was present, direct cation site occupancy refinements were performed on all data sets. Total occupancies were constrained to the stoichiometric composition. No measureable disorder was found at any temperature or pressure, with estimated standard deviations in the occupancies of ±1–2%. The observed mean bond distances of the octahedral sites are also consistent with complete order having been maintained under all conditions.

Temperature factors

Thermal ellipsoids calculated from all data collected at 1 atm pressure are presented in Table 8. Due to the paucity of intensity data, no attempt was made to refine anisotropic temperature factors for the high-pressure data.

Table 8. RMS amplitudes of vibration (Å) and orientation of thermal ellipsoids

	RTP*	24°C	400°C	600°C	800°C	1050°C	RTAH
Fe atom:							
Perpendicular to *c*	0.0876(6)	0.086	0.122	0.136(1)	0.150(1)	0.169(1)	0.085
Parallel to *c*	0.0916(9)	0.086	0.122	0.143(1)	0.160(1)	0.182(1)	0.085
Ti atom:							
Parallel to *c*	0.0841(10)	0.076	0.105	0.117(1)	0.126(2)	0.142(2)	0.077
Perpendicular to *c*	0.0778(6)	0.076	0.105	0.119(1)	0.131(1)	0.143(1)	0.077
Oxygen atom:							
Axis 1	0.0803(14)	0.077(2)	0.104(3)	0.118(3)	0.128(3)	0.143(4)	0.076(3)
Angle with *a*	52(11)**	28(6)	65(17)	33(74)	39(9)	74(25)	60(24)
Angle with *b*	70(10)	95(12)	63(9)	117(56)	82(7)	61(15)	71(15)
Angle with *c*	104(6)	78(15)	120(14)	57(67)	101(8)	130(13)	123(17)
Axis 2	0.0850(13)	0.082(2)	0.110(3)	0.120(3)	0.143(3)	0.148(3)	0.081(3)
Angle with *a*	41(11)	84(17)	141(14)	112(96)	59(10)	158(19)	144(22)
Angle with *b*	143(7)	126(5)	67(10)	118(55)	127(7)	61(15)	59(10)
Angle with *c*	64(5)	39(8)	129(13)	58(68)	41(8)	112(18)	125(18)
Axis 3	0.1003(13)	0.097(2)	0.132(3)	0.147(3)	0.160(3)	0.182(3)	0.099(3)
Angle with *a*	102(3)	117(4)	118(5)	113(4)	112(5)	105(4)	108(6)
Angle with *b*	60(3)	36(5)	37(4)	41(4)	38(7)	43(4)	38(5)
Angle with *c*	30(3)	54(5)	54(4)	49(4)	52(7)	48(3)	53(5)

*Crystal used for high-pressure study measured at room temperature and pressure.
**Angles given in degrees.

For the crystal studied at high temperature, thermal vibration of Fe and Ti was found to be essentially isotropic at room temperature and 400°C and only slightly anisotropic at higher temperatures. However, the room temperature and pressure refinement of the high-pressure crystal did indicate slightly anisotropic vibration of Fe and Ti, with the longer axes parallel to **c**. The oxygen ellipsoid was significantly anisotropic at all temperatures, with the direction of maximum vibration lying in the **a**–**c** plane, about 50-55° from **c** for the high-temperature crystal and 30° from **c** for the high-pressure crystal. The discrepancies between the two crystals at room temperature and pressure are not serious. Due to improved data collection procedures, we feel that the ellipsoids determined for the high-pressure crystal are probably somewhat more reliable.

Equivalent isotropic temperature factors (Hamilton, 1959) for the high-pressure crystal are slightly higher than those for the high-temperature crystal at room temperature. The B_{eq} for Ti increased linearly with temperature, whereas those for Fe and O increased more rapidly at higher temperatures. Isotropic temperature factors for all atoms were essentially unchanged with pressure.

Discussion

Mean Fe–O and Ti–O distances, uncorrected for thermal motion, increased linearly with temperature. The increase in ⟨Fe–O⟩ distance was twice as great as that for ⟨Ti–O⟩. Values of thermal expansion coefficients (Table 6) compare well with measured values of mean Fe^{2+}–O distances in fayalite (Smyth, 1975), wüstite (Carter, 1959), orthoferrosilite (Sueno *et al.*, 1976), and hedenbergite (Cameron *et al.*, 1973). The mean Ti^{4+}–O distance expansion was also comparable to values for this species reported for anatase (Horn *et al.*, 1972), rutile and brookite (Meagher and Lager, 1979), and titanite (Taylor and Brown, 1976). The lower rate of expansion for octahedral ⟨Ti^{4+}–O⟩ is consistent with the greater Pauling bond strength (cation charge/coordination number) of Ti^{4+}–O bonds. However, as was also pointed out by Meagher and Lager (1979), the expansion coefficients for ⟨Ti^{4+}–O⟩ distances are substantially greater than those expected from the trend pointed out by Hazen and Prewitt (1977).

The polyhedral bulk moduli, $K_p = 1/3\beta$ (Hazen and Finger, 1979), of the Fe and Ti sites in ilmenite are 1.4(1) and 2.9(5) Mbar, respectively. The Fe value compares well with values derived from compression of wustite (Clendenen and Drickamer, 1966; Will *et al.*, 1980) of about 1.6 Mbar. K_p for the Ti site is also consistent with the value of 2.2(8) reported by Hazen and Finger (1981) for TiO_2. The value determined in this study indicates that the TiO_6 polyhedron is among the least compressible octahedra yet found. The polyhedral bulk modulus for the Fe site is compatible with the semiempirical relation derived by Hazen and Finger (1979), although the Ti site has a somewhat smaller K_p than is predicted by this relation. Hazen and Finger (1981) also noted that K_p values for tetravalent ions show systematic deviations from the trend suggested by Hazen and Finger (1979).

The ilmenite structure is derived from the corundum structure by ordering of the octahedral sites into two nonequivalent layers. It is thus interesting to compare these results with those for R_2O_3 corundum structures reported by Finger and Hazen (1980). The compression in ilmenite is relatively anisotropic, with c/a decreasing about twice as rapidly as in Fe_2O_3, as compared with no change with pressure for Al_2O_3 and Cr_2O_3, and a rapid increase for V_2O_3. The decrease in c/a ratio and change in Fe coordinate in ilmenite are indicative of further departure from hexagonal close packing and the ideal corundum structure with increased pressure. However, this is partially offset by the changing oxygen y and z coordinates, which become more corundum-like at high pressure. Whereas the structural parameters for Fe_2O_3, Cr_2O_3, and Al_2O_3 remain essentially constant as pressure is increased, somewhat more distortion is observed in ilmenite, presumably due to the presence of two nonequivalent cation sites.

The bulk modulus and its pressure derivative are indicative of the mechanism of compression of crystal structures (Hazen and Finger, 1978). In a fully edge-linked structure such as that of ilmenite, the compressibility is expected to be mainly determined by shortening of M–O bonds. The fraction of the unit-cell volume occupied by the cation polyhedra in ilmenite is, in fact, constant between 1 atm and 46 kbar, as it is between 24 and 1050°C as well. Thus, although some distortion of the structure occurs under pressure, the overall rate of compression must be controlled by the compressibilities of the component polyhedra themselves. This being the case, it is reasonable to suggest that the actual K_o' for ilmenite is probably in the range of 4 to 5, as is observed in similar materials. Therefore, the bulk modulus determined with K_o' constrained to be 4(1), which gave $K_o = 1.77(3)$ Mbar (see above), may provide a slightly better estimate than the value determined with both K_o and K_o' allowed to vary ($K_o = 1.70(7)$, $K_o' = 8(4)$).

Some of the difference in compressional behavior between the Fe and Ti sites can perhaps be understood by considering the nature of the structure in the **a** and **c** directions. The ilmenite structure consists of alternating layers of edge-sharing Fe and Ti octahedra stacked along **c**. Compression along **a** is constrained by the more rigid polyhedron, *i.e.*, Ti, and both cation sites are compressed at virtually identical rates in this direction. Parallel to **c**, however, the two cation layers may be compressed more or less independently of one another. Therefore, differences between the overall volume compressibilities of the two sites may be expected to be expressed mainly in the **c** direction. Of course, this does not necessarily require a change in the c/a ratio unless one of the sites compresses equally in both directions, as Ti does in ilmenite. Similar

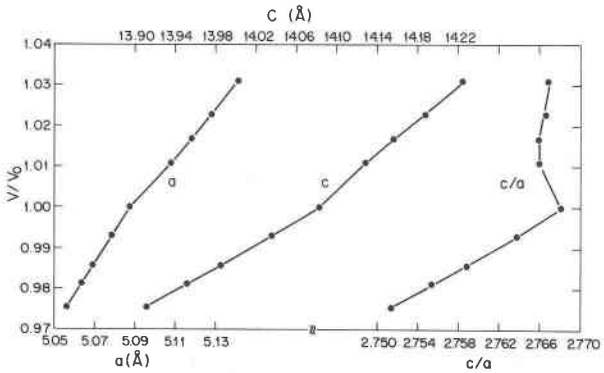

Fig. 1. Variation of ilmenite cell parameters with V/V_o.

behavior may also pertain to compression of other minerals having the ilmenite structure.

Comparison of temperature and pressure effects

Hazen and Prewitt (1977) suggested that in compounds where all component polyhedra have similar values of α/β, the mechanism of compression will be essentially equivalent to that of cooling, *i.e.*, compression and expansion have inverse effects. Although this criterion is satisfied in ilmenite, clearly the mode of compression is not the inverse of expansion. In Figure 1, a, c, and c/a are plotted against V/V_o (unit-cell volume at T, P divided by volume at 24°C, 1 atm). The striking difference between expansion and compression is clearly demonstrated by c/a. The linear decrease with pressure is contrasted with a small decrease followed by an even smaller increase with increasing temperature. Whereas the high-temperature behavior is characterized by nearly isotropic expansion of the unit cell and significant structural distortion, at high pressure the structural changes are smaller and the unit-cell compression is quite anisotropic.

Figure 2 demonstrates the linear relationship between mean Fe–O and Ti–O distances and V/V_o in ilmenite.

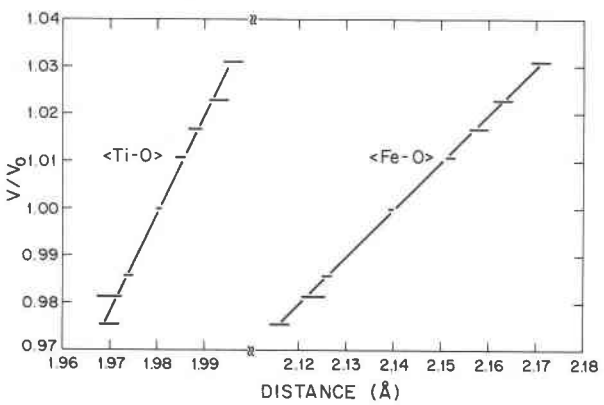

Fig. 2. Variation of mean Fe–O and Ti–O distances in ilmenite with V/V_o.

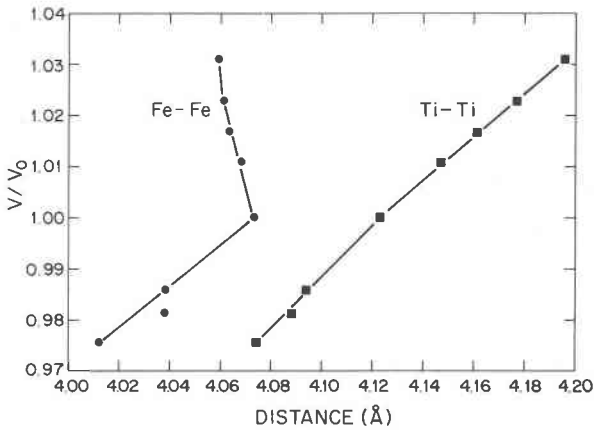

Fig. 3. Variation of Fe–Fe and Ti–Ti distances across vacant octahedral sites in ilmenite with V/V_o.

Thus, the difference between expansional and compressional behavior is not related to the mean M–O distances. It is interesting, however, to observe the individual bond distances which make up the coordination polyhedra. In both the Fe and Ti sites, the more expandable of the two independent M–O bonds are also the less compressible ones, the opposite of what might be expected if the rates of expansion and compression were proportional to individual bond strengths. The latter notion is reasonably useful when considering mean bond distances, however.

The oxygen coordinates vary approximately inversely with temperature and pressure, although changes in the cation coordinates are decidedly noninverse. As with increasing pressure, the octahedral height (along **c**) of the Fe layer probably changes much more rapidly than that of the Ti layer at high temperature. However, the net expansion along **c** is about equal to the expansion along **a**. This is perhaps due to metal–metal repulsion between adjacent Ti sites, resulting in increased separation and consequently greater expansion of the Ti layer along **a** than **c**.

The displacement of the Fe position at high temperature may also reflect the importance of metal–metal repulsions. The retreat of the Fe position away from the Ti across the shared face is suggestive of a significant repulsive interaction. This results in greater "puckering" of the Fe layer and an increase in Fe–Fe distances across shared edges. On the other hand, this shift also results in a decrease in the Fe–Fe separation across the vacant position along **c** at high temperature (Figure 3). Presumably the Fe–Fe interaction in this direction is weaker than the corresponding Ti–Ti repulsion, resulting in the tendency of the Fe site to distort in this fashion.

Acknowledgments

D. H. Lindsley provided the ilmenite crystals used in this study, and his thoughtful comments are appreciated. Assistance from and discussions with Kenneth Baldwin, Jay Bass, Benjamin Burton, Robert Hazen, Hubert King, Louise Levien, Robert

Liebermann, and Alexandra Navrotsky contributed measurably to the results. This research was supported in part by NSF Grant No. EAR81-20950.

References

Andersen, D. J. and Lindsley, D. H. (1979) The olivine–ilmenite thermometer. Proceedings of the Lunar and Planetary Science Conference, 10th, 493–507.

Barnett, J. D., Block, S., and Piermarini, G. J. (1973) An optical fluorescence system for quantitative pressure measurement in the diamond-anvil cell. Review of Scientific Instruments, 44, 1–9.

Barth, T. F. W. and Posnjak, E. (1934) The crystal structure of ilmenite. Zeitschrift für Kristallographie, A88, 265–270.

Bass, J. D., Liebermann, R. C., Weidner, D. J., and Finch, S. J. (1981) Elastic properties from acoustic and volume compression experiments. Physics of the Earth and Planetary Interiors, 25, 140–158.

Birch, F. (1966) Compressibility; elastic constants. In S. P. Clark, Jr., Ed., Handbook of Physical Constants, p. 97–173. Geological Society of America Memoir 97.

Bishop, F. C. (1980) The distribution of Fe^{2+} and Mg between coexisting ilmenite and pyroxene with applications to geothermometry. American Journal of Science, 280, 46–77.

Buddington, A. F. and Lindsley, D. H. (1964) Iron–titanium oxide minerals and synthetic equivalents. Journal of Petrology, 5, 310–357.

Burton, B. (1980) Crystallography of the ilmenite–corundum order–disorder transformation for an intermediate ilmenite–hematite solution. (abstr.) EOS, 61, 408.

Cameron, M., Sueno, S., Prewitt, C. T., and Papike, J. J. (1973) High-temperature crystal chemistry of acmite, diopside, hedenbergite, jadeite, spodumene, and ureyite. American Mineralogist, 58, 594–618.

Carter, R. E. (1959) Thermal expansion of $MgFe_2O_4$, FeO, and $MgO \cdot 2FeO$. Journal of the American Ceramic Society, 42, 324–327.

Clendenen, R. L. and Drickamer, H. G. (1966) Lattice parameters of nine oxides and sulfides as a function of pressure. Journal of Chemical Physics, 44, 4223–4228.

Doyle, P. A. and Turner, P. S. (1968) Relativistic Hartree–Fock X-ray and electron scattering factors. Acta Crystallographica, A24, 390–397.

El Goresy, A. (1976a) Oxide minerals in lunar rocks. In D. Rumble, Ed., Oxide Minerals, p. EG-1–EG-46. Mineralogical Society of America Short Course Notes, 3, Washington, D.C.

El Goresy, A. (1976b) Opaque oxide minerals in meteorites. In D. Rumble, Ed., Oxide Minerals, p. EG-47–EG72. Mineralogical Society of America Short Course Notes, 3, Washington, D.C.

Finger, L. W. and Hazen, R. M. (1980) Crystal structure and isothermal compression of Fe_2O_3, Cr_2O_3, and V_2O_3 to 50 kbars. Journal of Applied Physics, 51, 5362–5367.

Finger, L. W. and King, H. E., Jr. (1978) A revised method of operation of the single-crystal diamond cell and refinement of the structure of NaCl at 32 kbar. American Mineralogist, 63, 337–342.

Finger, L. W. and Prince, E. (1975) A system of FORTRAN IV computer programs for crystal structure computations. U. S. National Bureau of Standards Technical Note 854.

Finger, L. W., Hadidiacos, C. G., and Ohashi, Y. (1973) A computer-automated, single-crystal x-ray diffractometer. Carnegie Institution of Washington Year Book, 72, 694–699.

Haggerty, S. E. (1976) Opaque mineral oxides in terrestrial igneous rocks. In D. Rumble, Ed., Oxide Minerals, p. Hg-101–Hg-300. Mineralogical Society of America Short Course Notes, 3, Washington, D.C.

Hamilton, W. C. (1959) On the isotropic temperature factor equivalent to a given anisotropic temperature factor. Acta Crystallographica, 12, 609–610.

Hazen, R. M. and Finger, L. W. (1978) Relationships between crystal structure and compressibility in oxides and silicates. Carnegie Institution of Washington Year Book, 77, 848–850.

Hazen, R. M. and Finger, L. W. (1979) Bulk modulus–volume relationship for cation–anion polyhedra. Journal of Geophysical Research, 84, 6723–6728.

Hazen, R. M. and Finger, L. W. (1981) Bulk moduli and high-pressure crystal structures of rutile–type compounds. Journal of Physics and Chemistry of Solids, 42, 143–151.

Hazen, R. M. and Prewitt, C. T. (1977) Effects of temperature and pressure on interatomic distances in oxygen-based minerals. American Mineralogist, 62, 309–315.

Horn, M., Schwerdtfeger, C. F., and Meagher, E. P. (1972) Refinement of the structure of anatase at several temperatures. Zeitschrift für Kristallographie, 136, 273–281.

Ishikawa, Y. (1958) An order–disorder transformation phenomenon in the $FeTiO_3$–Fe_2O_3 solid solution series. Journal of the Physical Society of Japan, 13, 828–837.

Ishikawa, Y. (1962) Magnetic properties of the ilmenite–hematite system at low temperature. Journal of the Physical Society of Japan, 17, 1835–1844.

Ito, E. and Matsui, Y. (1979) High-pressure transformations in silicates, germanates, and titanates with ABO_3 stoichiometry. Physics and Chemistry of Minerals, 4, 265–273.

King, H. E., Jr. and Finger, L. W. (1979) Diffracted beam crystal centering and its application to high-pressure crystallography. Journal of Applied Crystallography, 12, 374–378.

King, H. E., Jr. and Prewitt, C. T. (1980) Improved pressure calibration system using the ruby R_1 fluorescence. Review of Scientific Instruments, 51, 1037–1039.

Kirfel, A., Hinze, E., and Will, G. (1978) The rhombohedral high-pressure phase of $MgGeO_3$ (ilmenite): synthesis and single-crystal structure analysis. Zeitschrift für Kristallographie, 148, 305–317.

Liebermann, R. C. (1976) Elasticity of ilmenites. Physics of the Earth and Planetary Interiors, 12, P5–P10.

Lindsley, D. H. (1963) Fe–Ti oxides in rocks as thermometers and oxygen barometers. Carnegie Institution of Washington Year Book, 62, 60–66.

Liu, L.-G. (1977a) The system enstatite–pyrope at high pressures and temperatures and the mineralogy of the Earth's mantle. Earth and Planetary Science Letters, 36, 237–245.

Liu, L.-G. (1977b) Ilmenite-type solid solutions between $MgSiO_3$ and Al_2O_3 and some structural systematics among ilmenite compounds. Geochimica et Cosmochimica Acta, 41, 1355–1361.

Liu, L.-G., Bassett, W. A., and Takahashi, T. (1974) Isothermal compressions of a spinel phase of Co_2SiO_4 and magnesian ilmenite. Journal of Geophysical Research, 79, 1171–1174.

Madelung, E. and Fuchs, R. (1921) Kompressibilitatsmessungen am festern korpers. Annalen der Physik (Berlin), 65, 289–309.

Meagher, E. P. and Lager, G. A. (1979) Polyhedral thermal expansion in the TiO_2 polymorphs: refinement of the crystal

structures of rutile and brookite at high temperature. Canadian Mineralogist, 17, 77–85.

Merrill, L. and Bassett, W. A. (1974) Miniature diamond anvil pressure cell for single crystal X-ray diffraction studies. Review of Scientific Instruments, 45, 290–294.

Piermarini, G. J., Block, S., and Barnett, J. D. (1973) Hydrostatic limits in liquids and solids to 100 kbar. Journal of Applied Physics, 44, 5377–5382.

Piermarini, G. J., Block, S., and Barnett, J. D. (1975) Calibration of the pressure dependence of the R_1 ruby fluorescence line to 195 kbar. Journal of Applied Physics, 46, 2774–2780.

Prince, E. (1978) A test of robust/resistant refinement on synthetic data sets. (abstr.) American Crystallographic Association. Program and Abstracts, 6, 37.

Raymond, K. N. and Wenk, H. R. (1971) Lunar ilmenite (refinement of the crystal structure). Contributions to Mineralogy and Petrology, 30, 135–140.

Ringwood, A. E. (1969) Phase transformations in the mantle. Earth and Planetary Science Letters, 5, 401–412.

Robinson, K., Gibbs, G. V., and Ribbe, P. H. (1971) Quadratic elongation: a quantitative measure of distortion in coordination polyhedra. Science, 172, 567–570.

Rumble, D. (1976) Oxide minerals in metamorphic rocks. In D. Rumble, Ed., Oxide Minerals, p. R-1–R-24. Mineralogical Society of America Short Course Notes, 3, Washington, D.C.

Sclar, C. B., Bauer, J. F., Pickart, S. J., and Alperin, H. A. (1973) Shock effects in experimentally shocked terrestrial ilmenite, lunar ilmenite of rock fragments in 1–10 mm fines (10085,19), and lunar rock 60015,127. Proceedings of the Lunar Science Conference, 4th, 1, 841–859.

Shirane, G., Pickart, S. J., Nathans, R., and Ishikawa, Y. (1959) Neutron diffraction study of antiferromagnetic $FeTiO_3$ and its solid solutions with α-Fe_2O_3. Journal of Physics and Chemistry of Solids, 10, 35–43.

Shirane, G. and Ruby, S. L. (1962) Mössbauer study of $FeTiO_3$ and its solid solutions with αFe_2O_3. Journal of the Physical Society of Japan, 17, Suppl. B-I, 133–135.

Shirane, G., Cox, D. E., Takei, W. J., and Ruby, S. L. (1962) A study of the magnetic properties of the $FeTiO_3$–Fe_2O_3 system by neutron diffraction and the Mössbauer effect. Journal of the Physical Society of Japan, 17, 1598–1611.

Smyth, J. R. (1975) High-temperature crystal chemistry of fayalite. American Mineralogist, 60, 1092–1097.

Sueno, S., Cameron, M., and Prewitt, C. T. (1976) Orthoferrosilite: High-temperature crystal chemistry. American Mineralogist, 61, 38–53.

Taylor, M. and Brown, G. E. (1976) High-temperature structural study of the $P2_1/a = A2/a$ phase transition in synthetic titanite, $CaTiSiO_5$. American Mineralogist, 61, 435–447.

Thorpe, A. N., Minkin, J. A., Senftle, F. E., Alexander, C., Briggs, C., Evans, H. T., and Nord, G. L., Jr. (1977) Cell dimensions and antiferromagnetism of lunar and terrestrial ilmenite single crystals. Journal of Physics and Chemistry of Solids, 38, 115–123.

Vaughan, R. W. and Drickamer, H. G. (1967) High-pressure Mössbauer studies on α-Fe_2O_3, $FeTiO_3$, and FeO. Journal of Chemical Physics, 47, 1530–1536.

Will, G., Hinze, E., and Nuding, W. (1980) The compressibility of FeO measured by energy dispersive X-ray diffraction in a diamond anvil squeezer up to 200 kbar. Physics and Chemistry of Minerals, 6, 157–167.

Manuscript received, August 11, 1982;
accepted for publication, July 22, 1983.